Impact of Polarization Impurity on Compact Antenna Array Receiver for Satellite Navigation Systems

S. Irteza[1], E. Schäfer[2], M. Sgammini[3], R. Stephan[1], M. A. Hein[1]
[1] RF and Microwave Laboratory, Ilmenau University of Technology, Germany
[2] Institut für Mikroelektronik- und Mechatronik-Systeme gemeinnützige GmbH, Germany
[3] German Aerospace Center (DLR), Institute for Communication and Navigation, Germany
Email: safwat-irteza.butt@tu-ilmenau.de

***Abstract*—We present a decoupled and matched four-element L1-band antenna array with an inter-element separation of a quarter of the free-space wavelength. We study the impact of polarization impurity in terms of the receiver's equivalent carrier-to-interference-plus-noise ratio when impinged with different numbers of diametrically polarized interferers. We observe that strong polarization impurity of the designed circular compact eigenmode antenna array, particularly for the high-order eigenmodes, reduces the available degrees-of-freedom for nulling by half in the presence of linear-polarized interferers with 40-dB interferer-to-signal power ratio.**

Keywords—compact, navigation, interferers, polarization, carrier-to-interference-plus-noise ratio

I. INTRODUCTION

Ensuring accurate and robust acquisition of position, velocity, and time in all environments is essential for future global navigation satellite systems (GNSS) applications in aviation, maritime, and consumer electronics. Therefore, in addition to higher bandwidth and dual-band operation, sophisticated beamforming algorithms for interference cancellation and multi-path mitigation are envisaged. This can be fulfilled with the use of a multi-element antenna. However, the resulting dimensions, due to a typical inter-element separation of half of the free-space wavelength, render such antennas unattractive. Reducing the inter-element separation, certainly lead to a compact antenna array design, but then it is impregnated with strong mutual coupling between the single elements, which degrades its performance significantly. This mutual coupling can be alleviated using a decoupling and matching network based on the eigenmode-excitation principle [1], [2]. With respect to this approach, exploitation of high-order, i.e. super-directive, modes is vital for multi-path and interference mitigation [3]. Since interferers and multi-path signals are obviously arbitrarily polarized, it is important to determine the influence of the polarization impurity of compact arrays on the navigation quality.

In navigation receivers, the available carrier-to-noise ratio (CNR) directly determines the navigation error. Therefore, a receiver model based on the noise characteristics of the environment, antenna array and front-end was introduced in order to derive the equivalent CNR as a figure-of-merit at the input of the first stage amplifier for compact antenna arrays [4].

In this paper, we extend this model with additional interferers. The interference can be treated as noise in terms of CNR degradation. Thus, a figure-of-merit, carrier-to-interference-plus-noise ratio (CINR), is derived. We employ it to analyze the performance of our four-element compact antenna array GNSS diversity receiver for different interfering scenarios. The interferer is assumed to be right-hand-circular polarized (RHCP), left-hand-circular polarized (LHCP), or linear polarized (LP), to determine the impact of polarization impurity, which may be a limiting factor defining the required degrees-of-freedom and the use of high-order modes in navigation receivers.

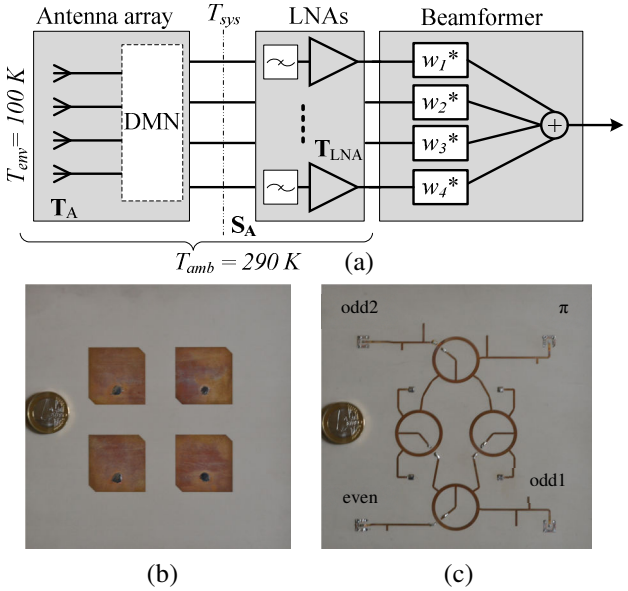

Fig. 1: (a) Receiver model. Furthere explaination in the text (b) Top view of the GNSS antenna array designed in this work. (c) DMN indicating the respective mode excitations, bottom view of the designed GNSS antenna array. The one-euro coin serves as visual size comparison.

II. GNSS DIVERSITY RECEIVER

The receiver model is depicted in Fig. 1 (a). DMN denotes the decoupling and matching network. $\mathbf{S}_A$ indicates the combined S-parameter matrix of antenna array and DMN. The conventional configuration excludes the DMN, which means, $\mathbf{S}_A$ reduces to the S-parameter matrix of the antenna array. $\mathbf{T}_A$ and $\mathbf{T}_{LNA}$ are the noise correlation matrices of the antenna array and the low-noise amplifiers, respectively. The equivalent CINR is obtained at the output of the null-constraint beamformer. Nonlinear effects due to analog-to-digital conversions are not considered for further discussion.

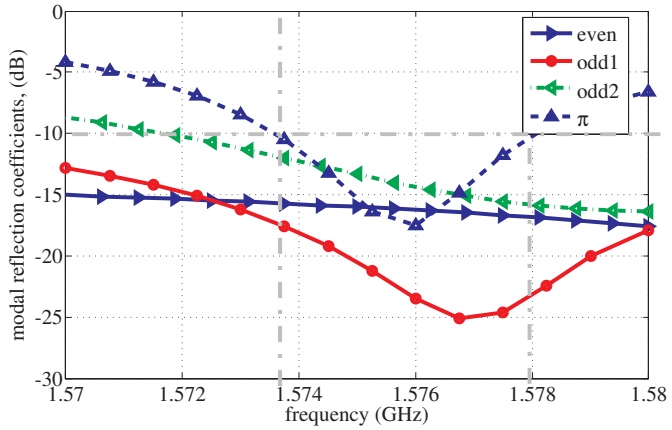

Fig. 2: Measured reflection or matching coefficients S_{ii} of the antenna array with DMN for respective modes. The grey highlighted lines indicate the required threshold for a L1-band navigation system.

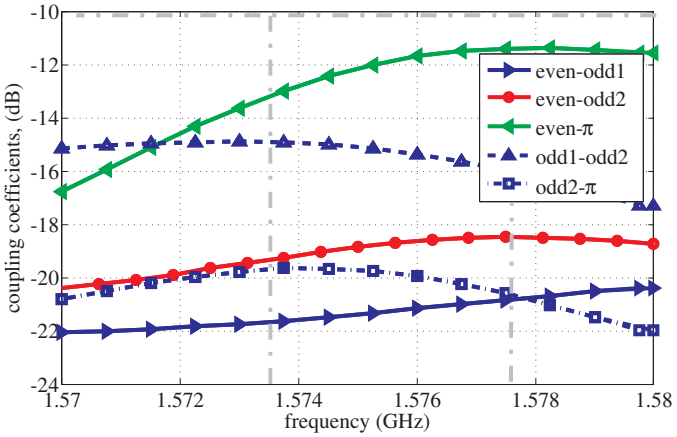

Fig. 3: Measured coupling coefficients S_{ij} of the antenna array with DMN among respective modes.

A. *Integrated Compact Antenna Array*

The antenna array comprises four truncated square patches [5], with an inter-element separation of a quarter of the free-space wavelength. The mutual coupling is mitigated using an integrated decoupling and matching network, which provides non-ideal eigenmode outputs. Non-ideality is due to the use of 180° hybrids for excitation of eigenvectors, which may not be the exact eigenvectors of the antenna array, and also the ohmic losses within the network. However, it maximizes the diversity performance diminished due to reduction of inter-element separation in comparison to without DMN case. The measured reflection coefficients at the output of the antenna array, including DMN, are shown in Fig. 2. All values are below −10 dB within a bandwidth of 4 MHz centered at 1575.42 MHz (L1-band center frequency). The coupling coefficients are below −15 dB, with an exception of S_{14} being smaller than −11 dB due to imperfect eigenmode decoupling using hybrids, see Fig. 3. This is acceptable but not ideal, and could be improved by more careful design and thinner network substrate.

The output modal RHCP radiation patterns are shown in Fig. 4 (a), along with LHCP radiation patterns in Fig. 4 (b). The measured total modal efficiencies are 64%, 56%, 35%, and 28%, respectively. The even mode has a maximum realized gain of 5.8 dBi and −5.8 dBi for RHCP and LHCP, respectively. In contrast, the π mode has a maximum gain of 0.2 dBi and −0.2 dBi for RHCP and LHCP, respectively. This suggest that high-order modes possess high levels of cross-polarization. Therefore, an arbitrarly polarized interferer may effect this RHCP array performance severly, which will be investigated in terms of the equivalent CINR using null-constraint beamformer in section III.

B. *Front End*

The front end consists of four independent low-noise amplifiers, each with a low-loss filter in front for better out-of-band interference rejection. The measured on-board noise parameters of the designed front-end channels are $F_{\min}$ = 1.66 dB, R_n = 8.2 Ω, and $|Z_{opt}|$ = 29 Ω, see [6],.

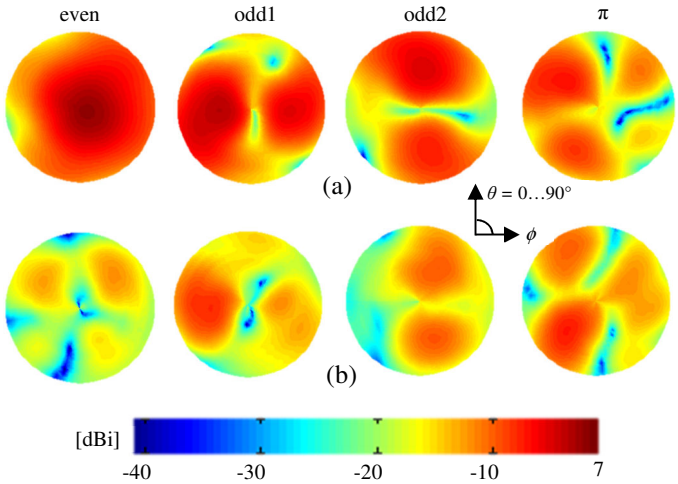

Fig. 4: (a) Measured realized gain RHCP patterns (polar maps) at the respective output ports of DMN for L1 frequency. The DMN is based on the principal of eigenmode excitation, and, therefore, each pattern represents a mode. (b) Measured realized gain cross polarization or LHCP patterns at the respective output ports of the DMN.

C. *Beamforming*

To assess the equivalent CINR, a modified version of the well-known null-constraint beamformer [7], differing in the selection of the zero-order constraints, is considered. The optimum weighting coefficients are obtained using:

$$\mathbf{w} = \mathbf{w}_d^H - (\mathbf{w}_d^H \mathbf{w}_I (\mathbf{w}_I^H \mathbf{w}_I)^{-1} \mathbf{w}_I^H), \quad (1)$$

where $\mathbf{w}_d$ is the eigenmode vector response in the desired direction of the signal, $\mathbf{w}_I$ is defined as the null-constraint matrix for the unwanted direction of interferers, with the columns representing the interferer.

III. Equivalent Carrier-to-Interference-Plus-Noise Ratio

The equivalent available carrier power is calculated from

$$C(\phi,\theta) = C_{sat} \mathbf{w}^H \mathbf{f}_{RHCP}(\phi,\theta) \mathbf{f}_{RHCP}^H(\phi,\theta) \mathbf{w}, \quad (2)$$

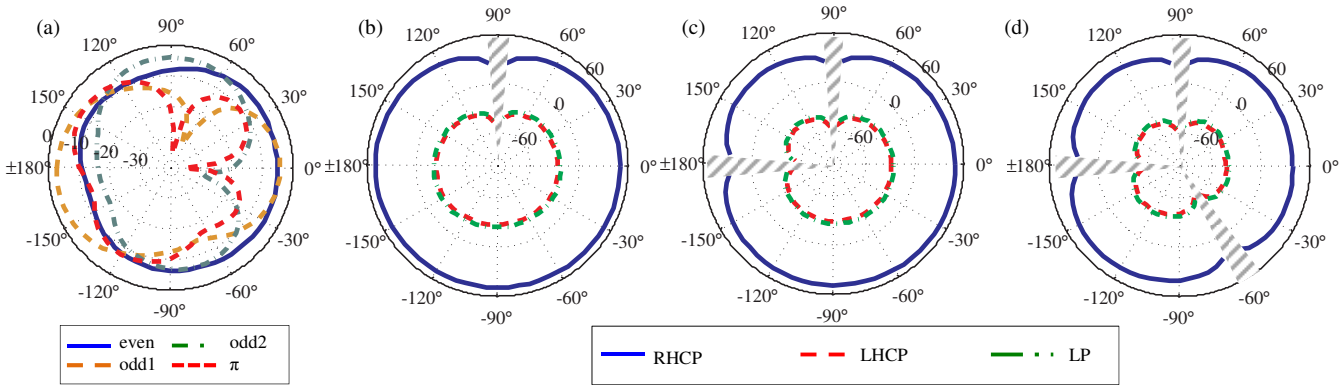

Fig. 5: (a) Measured realized gain modal RHCP ϕ-cuts at $\theta = 60°$, normalized to maxima of even mode. ϕ-cut at $\theta = 60°$ for the calculated CINR in dBHz (b) for one interferer, (c) two interferers, and (d) three interferers. Shaded region indicate blind region for beamforming algorithm, when interferer is in the direction of desired signal.

C_{sat} is the power received with an ideal RHCP isotropic antenna, and $\mathbf{w}$ is the vector of the weighting coefficients in the deterministic beamformer. The individual elements of the column vector $\mathbf{f}_{\text{RHCP}}(\phi,\theta)$ denote the normalized complex-valued realized RHCP amplitude gain of the single antennas with respect to an isotropic radiator [1].

We derive the noise power spectral density from the equivalent system noise temperature T_{sys}, referred to the LNA inputs:

$$N_o = k_{\text{B}} T_{\text{sys}} = k_{\text{B}} \underbrace{\mathbf{w}^{\text{H}} \mathbf{T}_{\text{A}} \mathbf{w}}_{T_{\text{A}}} + k_{\text{B}} \underbrace{\frac{\mathbf{w}^{\text{H}} \mathbf{T}_{\text{LNA}} \mathbf{w}}{\mathbf{w}^{\text{H}} \left(\mathbf{I} - \mathbf{S}_{\text{A}} \mathbf{S}_{\text{A}}^{\text{H}} \right) \mathbf{w}}}_{T_{\text{LNA}}}. \quad (3)$$

$\mathbf{T}_{\text{A}}$ and $\mathbf{T}_{\text{LNA}}$ are computed according to [4]. The equivalent available interference power is defined as

$$I(\phi,\theta) = I_{\text{int}} \mathbf{w}^{\text{H}} \mathbf{f}_{\text{RHCP}}(\phi,\theta) \mathbf{f}_{\text{RHCP}}^{\text{H}}(\phi,\theta) \mathbf{w} \quad (4)$$

for a RHCP interferer,

$$I(\phi,\theta) = I_{\text{int}} \mathbf{w}^{\text{H}} \mathbf{f}_{\text{LHCP}}(\phi,\theta) \mathbf{f}_{\text{LHCP}}^{\text{H}}(\phi,\theta) \mathbf{w} \quad (5)$$

for a LHCP interferer, and

$$I(\phi,\theta) = \frac{1}{2} I_{\text{int}} \left(\mathbf{w}^{\text{H}} \mathbf{f}_{\text{RHCP}}(\phi,\theta) \mathbf{f}_{\text{RHCP}}^{\text{H}}(\phi,\theta) \mathbf{w} + \mathbf{w}^{\text{H}} \mathbf{f}_{\text{LHCP}}(\phi,\theta) \mathbf{f}_{\text{LHCP}}^{\text{H}}(\phi,\theta) \mathbf{w} \right) \quad (6)$$

for a LP interferer. I_{int} is the power received from the interferer by an ideal co-polarized isotropic antenna. This leads to the equivalent carrier-to-interference-plus-noise ratio

$$CINR(\phi,\theta) = \frac{C(\phi,\theta)}{\sum_i I(\phi_i,\theta_i) + N_o}. \quad (7)$$

IV. Interference Cancellation

The measured gain RHCP ϕ-cut is shown for all modes in Fig. 5 (a). The even-mode gain is uniform over the azimuth with no nulls. However, the π mode, i.e. the highest-order mode, possesses the maximal number of nulss (here: 3) nulls with a depth up to −40 dB.

Now, in order to evaluate the antenna performance for GNSS applications, C_{sat} is considered to be −157 dBW [8]. Then, the desired signal direction-of-arrival (DoA) is steered across the upper hemisphere while the directions-of-interference (ϕ_i, θ_i) are kept fixed. The weighting-coefficient vector $\mathbf{w}$ for every DoA is applied to (2)-(6), in the end the CINR using (7) is calculated for the respective DoA. Due to numerical limitation, the equivalent CINR cannot be calculated in directions-of-interference.

We consider different scenarios with different number of arbitrary polarized interferer for evaluation of the antenna array. In these scenarios, the equivalent received power of each interferer is fixed to −117 dBW at an isotropic antenna with the same polarization, which is 40 dB higher than the signal power.

A. Single Interferer

A single interferer, either RHCP, LHCP, or LP, fixed at $\phi_i = 90°$, $\theta_i = 60°$ is projected upon the antenna array. The subsequent CINR ϕ-cut for all three cases is shown in Fig. 5 (b). Since nulling and desired-direction constraints are calculated with respect to RHCP only, the beamformer clearly leads to optimal CINR values only in the situation of a RHCP interferer, whereas a LHCP or a LP interferer degrades the performance. In this case the maximum CINR drops below 0 dB, which is about 75 dB below the RHCP case. We can certainly use additional degrees-of-freedom in null-constraint matrix; this scenario is discussed later in this section.

B. Two Interferers

In the second scenario, we study the illumination with two interferers, fixed at $\phi_i = 90°$, 180°, $\theta_i = 60°$ of either RHCP, LHCP, or LP. The CINR in case of RHCP interferers is again quite high, as revealed in Fig. 5 (c). The maximum CINR is slightly lowered by 0.5 dB compared to a single RHCP interferer, which is still acceptable. In case of LHCP or LP interferers, the CINR in the desired directions is severely impaired, due to high cross polarization content in high-order modes.

C. Three Interferers

The maximum number of interferers that can be mitigated using a four-element antenna array is three, with one degree-

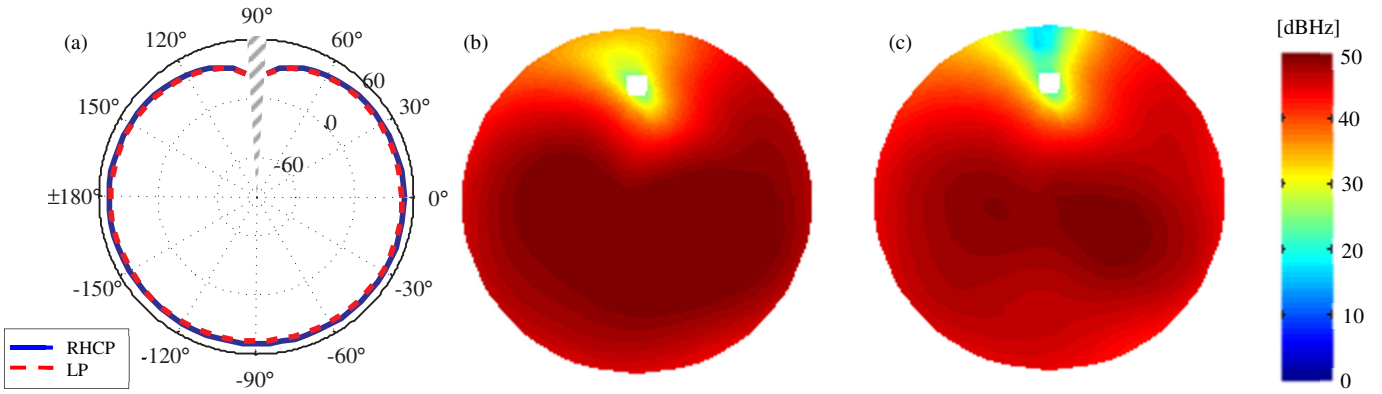

Fig. 6: Calculated CINR in dBHz for one interferer, with multiple-constraint beamforming algorithm. (a) ϕ-cut at $\theta = 60°$, (b) RHCP interferer (upper-hemisphere), and (c) LP interferer (upper-hemisphere).

of-freedom used for desired direction. This is the worst case since it mainly relies on exploitation of the π-mode, which is most strongly affected by mutual coupling. The RHCP, LHCP, or LP interferers are fixed at $\phi_i = 90°, 180°, 360°$, $\theta_i = 60°$. The ϕ-cut of the CINR curve is shown in Fig. 5 (d). It clearly indicates the superior performance of the RHCP-interferer case. The maximum CINR decreases by at least 6 dB in contrast to a single-RHCP interferer situation.

D. Maximum Degrees-of-Freedom for Nulling

If we employ an additional LHCP null-constraint in the previously considered single-LP interferer situation, we bind one of the remaining two degrees-of-freedom for suppression of another LHCP interferer. For the case that RCHP and LHCP constraint are nulling the same direction-of-arrival, LP interferes can be also mitigated. With this configuration we achieve a similar CINR performance in all azimuth directions as compared to a single RHCP interferer.

The CINR patterns calculated for our compact antenna are shown in Fig. 6 (a), the polar plot in the complete upper-hemisphere for one RHCP and one LP interferer is shown in Fig. 6 (b) and (c), respectively. The CINR with RHCP interferer seems to be slightly better than with LP interferer, especially at directions close to direction of the interference. However, the maximum CINR does not suffer significantly with the additional nulling constraint. Since there is still one degree-of-freedom unbound, another null-constraint can be incorporated. For our four-element circularly polarized compact antenna array, this approach of interference cancellation will ensure nullification of maximum one arbitrarily polarized interferer and either one RHCP or one LHCP interferer.

V. CONCLUSIONS

We have investigated the robustness of a four-element compact antenna array under influence of the arbitrarily polarized interference in terms of the equivalent CINR. The designed compact antenna array with the use of null-constraint beamformer can null-out three RHCP interferers perfectly, and is able to maintain a higher CINR in the desired direction. However, it is observed that elevated cross-polarization content for high-order modes, requires extra degrees-of-freedom to cancel the LP interferences completely. The designed array in the case of chosen null-steering technique is capable of mitigating either one LP and one CP interferer or three CP interferers. If more interference cancellation is desired either more or dual-polarized elements should be incorporated. Here, the question arises how many numbers of interferer cancellation are adequate? In case of the compact arrays more number of elements lead to inefficient degrees-of-freedom and will lower the CINR significantly, due to the increased mutual coupling. Therefore, a trade-off between number of elements and compactness can be made for a certain CINR threshold, especially in GNSS applications for an arbtirarily polarized interference environment.

ACKNOWLEDGMENT

We gratefully acknowledge M. Huhn and M. Zocher for their technical assistance. The authors would also like to thank Dr. A. Dreher and Dr. C. Volmer for their valuable suggestions and discussions in this work. This work was supported by the German Aerospace Center (DLR) on behalf of the German Federal Ministry of Economics and Technology under Grant 50 NA 1007.

REFERENCES

[1] S. Irteza, N. Murtaza, S. Caizzone, R. Stephan, M. A. Hein, "Compact planar L-band antenna arrays with optimal diversity performance," *IEEE Topical Conference on Antennas and Propagation in Wireless Communications*, Torino, Italy, Sep. 2011.

[2] C. Volmer, *Compact antenna arrays in mobile communications: A quantitative analysis of radiator coupling*, Ilmenau: Universitätsverlag Ilmenau, 2010.

[3] N. Basta *et al.*, "System concept of a compact multi-antenna GNSS receiver," *7th German Microwave Conference*, Ilmenau, Germany, Mar. 2012.

[4] S. Irteza *et al.*, "Noise Characterization of a Multi-Channel Receiver Using a Small Antenna Array with Full Diversity for Robust Satellite Navigation," *IEEE International Conference on Wireless Information Technology and Systems*, Maui (HI), USA, Nov. 2012.

[5] C. A. Balanis, *Antenna Theory: Analysis and Design*, 2nd ed. New York: John Wiley & Sons, 1997.

[6] J. Engberg and T. Larsen, *Noise Theory of Linear and Nonlinear Circuits*, Chichester: John Wiley & Sons, 1995.

[7] H. L. Van Trees, *Optimum Array Processing - Part IV of Detection, Estimation and Modulation Theory*, New York: John Wiley & Sons, 2002.

[8] Galileo OS SIS ICD. [Online]. Available: http://ec.europa.eu/-enterprise/policies/satnav/galileo/files/galileo-os-sis-icd-issue1-revision1_en.pdf